Acta Crystallographica Section B
Structural Science, Crystal Engineering and Materials
ISSN 2052-5192

Single-crystal metastable high-temperature *C*2/*c* clinoenstatite quenched rapidly from high temperature and high pressure

Akira Yoshiasa,[a]* Akihiko Nakatsuka,[b]‡ Maki Okube[c] and Tomoo Katsura[c]§

[a]Graduate School of Science and Technology, Kumamoto University, Kumamoto 860-8555, Japan, [b]Graduate School of Science and Engineering, Yamaguchi University, Ube 755-8611, Yamaguchi, Japan, and [c]Institute for Study of the Earth's Interior, Okayama University, Misasa 682-0193, Tottori, Japan

‡ Present address: Materials and Structures Laboratory, Tokyo Institute of Technology, 226-850 Yokohama, Kanagawa, Japan.
§ Present address: Bayerisches Geoinstitut, University of Bayreuth, 95440 Bayreuth, Germany.

Correspondence e-mail: yoshiasa@sci.kumamoto-u.ac.jp

Received 28 March 2013
Accepted 14 October 2013

The high-temperature clinoenstatite (HT-CEn) is one of the most important $MgSiO_3$ pyroxene polymorphs, but the details of its structure and stability have been uncertain. The single crystal of the *C*2/*c* HT-CEn end-member is firstly synthesized by rapid pressure–temperature quenching from 15–16 GPa and 1173–2173 K. The single-crystal X-ray diffraction analysis shows unusual bonding distances and static disorder of the atoms frozen in this metastable structure. The degree of kinking of the silicate tetrahedral chains is 175° for HT-CEn. The chain angle for HP-CEn is substantially smaller (135°), but the angle for L-CEn is in the opposite direction at −160° (= 200°). The degree of kinking increases by being curved by more than 180° for the transition from HT-CEn to L-CEn. As for the reverse change from the expansion to the stretch, a potential barrier exists at the point of the continuity. It is suggested that the reason why a structure can be quenched under ambient conditions is as follows: the present HT-CEn single crystal has been formed by the isosymmetric phase transition from the high-pressure *C*2/*c* clinoenstatite (HP-CEn). The presence of HT-CEn from HP-CEn in natural rocks is an indicator of quenching history, which leads to the possibility that it exists in shocked meteorites and impact materials.

1. Introduction

Minerals with the pyroxene stoichiometry $MgSiO_3$ are among the important constituents of the Earth's crust, upper mantle and meteorites. The transition of pyroxenes to denser garnet structures is believed to be a possible cause of the seismic discontinuity at a depth of 400 km of the Earth's mantle (Ringwood, 1967; Akaogi & Akimoto, 1977; Ito & Takahashi, 1987). Five different structure forms are well known in $MgSiO_3$ pyroxene: orthoenstatite (OEn) with the space group *Pbca*, protoenstatite (PEn) with *Pbcn*, low-temperature clinoenstatite (L-CEn) with $P2_1/c$, high pressure clinoenstatite (HP-CEn) with *C*2/*c* and high-temperature clinoenstatite (HT-CEn) with *C*2/*c*. Fig. 1 shows the temperature and pressure relationship of these phases (Presnall & Gasparik, 1990; Yusa *et al.*, 1993; Angel & Hugh-Jones, 1994). β-OEn (Zhang *et al.*, 2012) and γ-OEn (Jahn, 2008) have been described and their transformations have been studied very recently by Dera *et al.* (2013). The stable phase at ambient pressure and temperature is L-CEn (Angel *et al.*, 1992; Jiang *et al.*, 2002). The high-pressure and high-temperature stable phase HP-CEn transforms into L-CEn at low pressure and low temperature (Angel *et al.*, 1992). HP-CEn is unquenchable to ambient conditions; the transition from HP-CEn to L-CEn is reversible by pressure, but with significant hysteresis at room temperature (Angel & Hugh-Jones, 1994). HT-CEn was reported to be a

Table 1
Chemical compositions of recovered single-crystal specimens.

	Sample 1	Sample 2	Sample 3	Sample 4	Sample 5	Sample 6
Element (wt%)						
Na_2O	–	–	0.04	0.07	–	–
MgO	40.00	40.08	40.03	39.85	40.20	40.59
Al_2O_3	–	–	–	–	0.14	0.27
SiO_2	59.33	59.57	59.28	59.28	59.51	58.86
Total	99.33	99.65	99.35	99.20	99.85	99.72
Cation						
Na	–	–	0.01	0.01	–	–
Mg	4.00	3.99	4.01	4.00	4.01	4.07
Al	–	–	–	–	0.01	0.02
Si	4.00	4.00	3.99	4.00	3.99	3.95
Total	8.00	7.99	8.01	8.01	8.01	8.04

*C*2/*c* polymorph which is different from HP-CEn, and is thought to occur only at low pressure and high temperatures (Smyth, 1969; Angel *et al.*, 1992). It has been predicted based on the molecular dynamics (MD) simulation (Shimobayashi *et al.*, 1998) that HP-CEn undergoes a first-order phase transition to HT-CEn by decompression at high temperature. The transition maintains the approximate unit cell and the same space group with discontinuous volume change (the isosymmetric phase transition, see Christy, 1995). Details of the HT-CEn end-member were uncertain in the pyroxene polymorphs, only the possibility of its presence had been pointed out (Bowen & Schairer, 1935; Gasparik, 1990; Shimobayashi & Kitamura, 1991, 1993; Iishi & Kitayama, 1995; Jiang *et al.*, 2002). Almost all studies observed the subsidiary appearance of HT-CEn at high temperature and ambient pressure. Some of the previous studies (Bowen & Schairer, 1935; Gasparik, 1990; Iishi & Kitayama, 1995) reported that HT-CEn was a stable phase. However, no report has been made on the $MgSiO_3$ end-member that it is produced as a single crystal or a large domain. Its crystal structure has not been defined and the transition mechanism remains unknown experimentally to date. The HT-CEn-type modifications are observed in Ca-poor Mg–Fe clinoenstatite and pigeonite and they are always found to be unquenchable in rapid cooling (Smyth, 1974; Cámara *et al.*, 2002). However, these studies have not provided detailed structural data for the HT-CEn polymorph (Tribaudino *et al.*, 2002; Alvaro *et al.*, 2011). It is therefore surprising that single crystals of pure Mg end-member with HT-CEn topology can be obtained under room conditions.

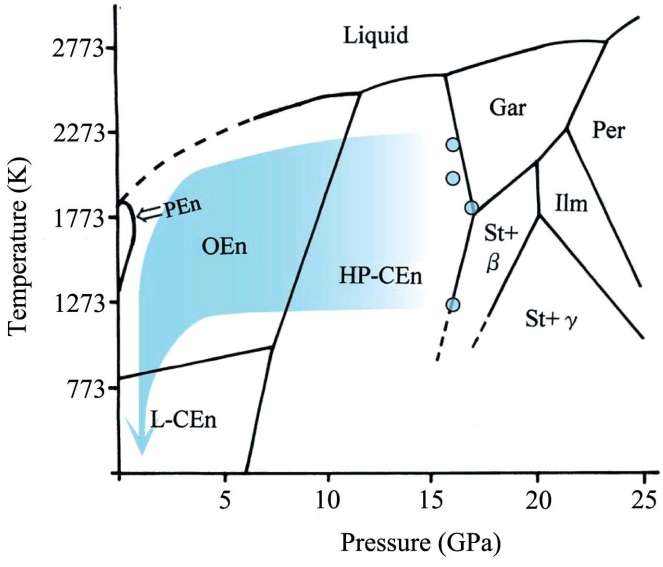

Figure 1
The phase diagram of $MgSiO_3$ based on previous studies (Presnall & Gasparik, 1990; Yusa *et al.*, 1993; Angel & Hugh-Jones, 1994). HT-CEn crystals were confirmed in all the samples recovered, formed by quenching from the pressures and temperatures indicated by circles in the figure. The predicted quenching route from HP-CEn is shown by the shaded arrow.

2. Experimental

The high-pressure and high-temperature experiments of $MgSiO_3$ were carried out with a Kawai-type multi-anvil apparatus (Kawai *et al.*, 1973). Special grade reagents of MgO and SiO_2 were used as the starting materials. These oxides were mixed in the stoichiometric molar ratio $MgO:SiO_2 = 1:1$ together with 15 mol% of PbO flux (sample 1 and 2 in Table 1). The starting composition with added Na and Al (several percent) was also tried (samples 3–6 in Table 1), as in the case of Na-majorite garnets (Nakatsuka, Yoshiasa, Yamanaka & Ito, 1999; Nakatsuka, Yoshiasa, Yamanaka, Katsura & Ito, 1999). In the high-pressure and high-temperature experiments, temperature was elevated after a gradual increase in pressure. The sample temperature and pressure were monitored by a thermocouple and load pressure, respectively. When pressure and temperature reached those shown in Fig. 1, the samples were quenched by rapidly releasing the oil pressure load and/or by a blow out of the anvil cell gasket. HT-CEn crystals were confirmed from all of these recovered samples. Table 1 shows the chemical compositions of the recovered single-crystal specimens obtained using a JEOL JCMA-733II electron microprobe analyzer. The beam diameter was 5 µm. The standards for Na, Mg, Al, Si and Pb were albite, periclase, corundum, quartz and galena, respectively. *ZAF* corrections, which correct for atomic number (*Z*), absorption (*A*) and fluorescence (*F*), were made. No contamination of Pb into the crystal was detected. Trace amounts of Na or Al were detected and both ions essentially were not contained in the crystals.

The $MgSiO_3$ single crystal (sample 1 in Table 1) of dimensions 100 × 100 × 120 µm was picked up from a run product obtained by rapidly releasing the oil pressure load from 16 GPa and 2173 K and it was used for the structure analysis. The space group *C*2/*c* was strictly determined by Rigaku RAPID Weissenberg photographs and synchrotron radiation

Table 2
X-ray data for high-temperature clinoenstatite ($MgSiO_3$).

Crystal data	
Chemical formula	Mg_2O_6
M_r	200.78
Crystal system, space group	Monoclinic, $C2/c$
Temperature (K)	296
a, b, c (Å)	9.5387 (8), 8.6601 (7), 5.2620 (4)
β (°)	108.701 (6)
V (Å^3)	411.73 (6)
Z	4
Radiation type	Mo $K\alpha$
μ (mm^{-1})	1.11
Crystal size (mm)	0.12 × 0.10 × 0.10
Data collection	
Diffractometer	Rigaku AFC7R
Monochromator	Graphite
Scan method	ω–2θ scans
Scan speed (° min^{-1})	4 in 2θ
Absorption correction	None
No. of measured, independent and observed ($F > 3\sigma F$) reflections	4535, 2171, 766
R_{int}	0.015
$(\sin\theta/\lambda)_{max}$ (Å^{-1})	1.078
Refinement	
$R[F^2 > 2\sigma(F^2)]$, $wR(F^2)$, S	0.029, 0.020, 1.51
No. of reflections	766
No. of parameters	48
$\Delta\rho_{max}$, $\Delta\rho_{min}$ (e Å^{-3})	0.73, −1.05

Computer programs: *WinAFC* Version 1.03 (Rigaku Corporation, 1999), *RADY* (Sasaki, 1987), *VESTA* (Momma & Izumi, 2006).

at beamline BL-10A of PF, KEK (Yoshias, 2001). Single-crystal X-ray diffraction experiments were performed at ambient conditions using a four-circle diffractometer (Rigaku AFC-5). A total of 9383 reflections were measured and averaged in Laue symmetry $2/m$ to give 766 independent reflections with $|F_o| \geq 3\sigma(|F_o|)$ used for the structure refinements. The structure refinements were carried out using the full-matrix least-squares program *RADY* (Sasaki, 1987). Final reliability factors converged smoothly to $R = 0.029$ and $wR = 0.020$. After the final refinement (Table 2 and supplementary material[1]), no significant residual electron density was detected in the difference-Fourier maps.

3. Results and discussion

3.1. Structure, formation of a single-crystal HT-CEn and isosymmetric phase transition

We estimate that the transitions from HP-CEn to L-CEn *via* HT-CEn are displacive type transitions that maintain the approximate unit cell and involve the simultaneous rotation of all the chains present in the structure. HT-CEn and HP-CEn have the same space group of $C2/c$, but greatly different β angles of 109 and 101°, respectively (Shimobayashi *et al.*, 1998). In Fig. 2 the HT-CEn and L-CEn structures obtained by single-crystal diffraction experiments at ambient conditions are shown in comparison to the HP-CEn structure (Angel *et al.*, 1992) determined under high pressure. The structures of the $MgSiO_3$ pyroxene polymorphs are characterized by chains of corner-sharing SiO_4 tetrahedra and edge-sharing MgO_6 octahedra, and these chains run parallel to the c axis. These three polymorphs of clinoenstatite share the same stacking sequence of $Mg1O_6$ octahedral strips. The most striking differences among HT-CEn, HP-CEn and L-CEn are in the different degree of kinking of the silicate tetrahedral chains. HP-CEn has the extremely kinked SiO_4 tetrahedral chains, whose chain angle (defined as the $O3^2-O3^3-O3^2$ angle in Fig. 2) is substantially smaller (∼ 135°) than the ∼ 175° for HT-CEn and the ∼ 200° (= −160°: reverse rotation) for L-

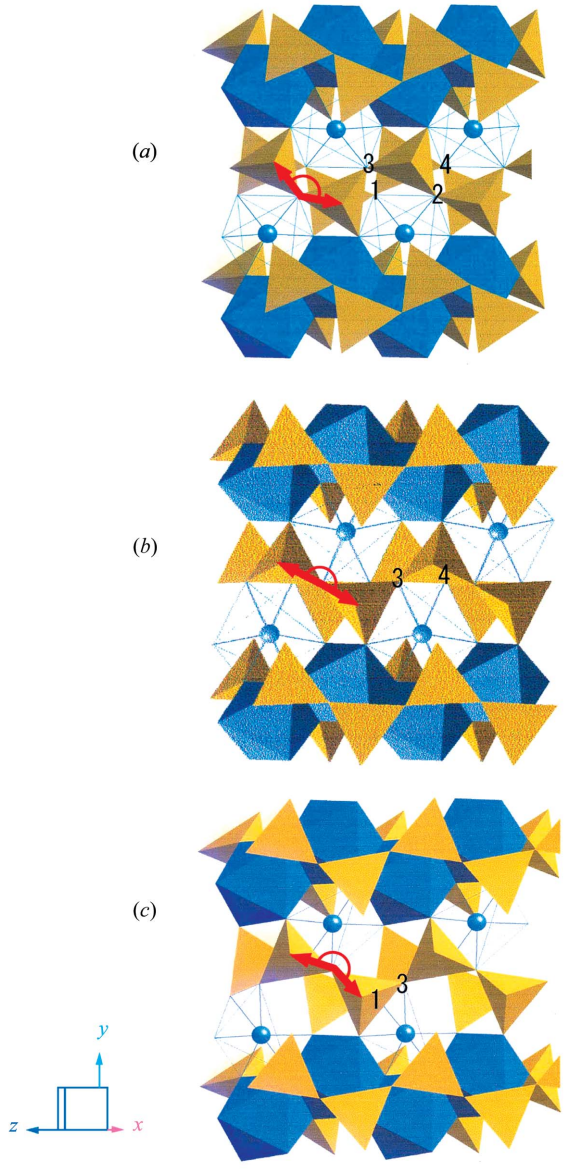

Figure 2
Comparison of the crystal structures among (*a*) HT-CEn, (*b*) HP-CEn (Angel *et al.*, 1992) and (*c*) L-CEn (Morimoto *et al.*, 1960). $Mg1O_6$ and SiO_4 sites are shown by tetrahedral and octahedral descriptions, respectively. The spheres represent the Mg2 ions. Each coordination environment around the Mg2 site can be distinguished by the bonding to the O3 atoms labeled in Nos. 1–4.

[1] Supplementary data for this paper are available from the IUCr electronic archives (Reference: BP5052). Services for accessing these data are described at the back of the journal.

Table 3
Cell dimensions and cell volumes of enstatite polymorphs and diopside.

Name	a (Å)	b (Å)	c (Å)	β (°)	V (Å^3)	T or P	c/b
High-T CEn[a]	9.5387 (8)	8.6601 (7)	5.2620 (4)	108.701 (6)	411.73 (6)	RT	0.6076
Low CEn[b]	9.606 (1)	8.815 (1)	5.169 (1)	108.33 (1)	415.5 (1)	RT	0.5863
High-P CEn[c]	9.201 (3)	8.621 (1)	4.908 (1)	101.20 (3)	381.5 (3)	7.9 GPa	0.5693
Orthoenstatite[d]	18.225 (1)	8.815 (1)	5.175 (1)	90.0	831.3 (1)	RT	0.5871
Protoenstatite[e]	9.252 (2)	8.740 (1)	5.316 (1)	90.0	429.9 (1)	RT	0.6082
High-T CEn (Ca) ($Ca_{0.15}Mg_{1.85}Si_2O_6$)[f]	9.885 (6)	8.978 (3)	5.339 (3)	110.03 (3)	445.2 (4)	1373 K	0.6014
Diopside[g]	9.746 (4)	8.899 (5)	5.251 (6)	105.63 (6)	438.6 (3)	RT	0.5901

References: (*a*) This study; (*b*) Morimoto *et al.* (1960); (*c*) Angel *et al.* (1992); (*d*) Ohashi (1984); (*e*) Murakami *et al.* (1984); (*f*) Tribaudino *et al.* (2002); (*g*) Cameron *et al.* (1973).

CEn. The degree of kinking decreases and the tetrahedral chain expands most in the transition from HP-CEn to HT-CEn. On the other hand, the degree of kinking increases by being curved by more than 180° in the transition from HT-CEn to L-CEn (*e.g.* $O3^2—O3^3—O3^2$ angle of $\sim 200° = -160°$). As for the reverse change from the expansion to the stretch at 180°, a potential barrier exists at the point of the continuity. The transitions from HP-CEn to L-CEn *via* HT-CEn involve displacements of the O3 atom positions with rotation of the tetrahedra in the silicate chain; these transitions involve the break and recombination of the Mg2—O3 bond. Each coordination environment around the Mg2 site can be distinguished by the bonding to the O3 atoms labeled by Nos. 1–4 in Fig. 2. The same mechanism is also observed in pegeonite (Cámara *et al.*, 2002; Alvaro *et al.*, 2010).

The crystal of HP-CEn transforms into the single-crystal HT-CEn because of the continuous kinking of the tetrahedral chain and the fast structure change by recombining the Mg2—O3 bonds. In the OEn stable region, HP-CEn and HT-CEn does not rapidly transform into OEn because the transitions into OEn are of reconstructive type that involves breaking of strong bonds, rearranging of the chain structure and changes to the stacking sequence. As the transitions of HP-CEn and HT-CEn to OEn are sluggish, HP-CEn transforms to metastable HT-CEn during passing through the wide stable area of OEn. This is probably the reason why HT-CEn can be quenched through the high-temperature regions in which the atomic thermal motion is large.

At room pressure, the HT-CEn-type modifications were always found to be unquenchable by rapid cooling in Ca-poor Mg–Fe clinopyroxenes (Smyth, 1974; Cámara *et al.*, 2002) and in other particular compositions such as kanoite (Arlt & Armbruster, 1997), ferric magnesian spodumene (Cámara *et al.*, 2003) or a large variety of other synthetic compositions involving only trivalent cations at *M*1 and monovalent cations at *M*2 (Redhammer & Roth, 2004), as well as clinopyroxenes germanates (Redhammer *et al.*, 2010). A single crystal of the *C*2/*c* HT-CEn $MgSiO_3$ end-member was firstly stabilized at room temperature by rapid pressure–temperature quenching. As discussed above, it is concluded that an important point is the transition mechanism from the HP-CEn phase. The degree of kinking decreases and the tetrahedral chain angle expands most in the transition from HP-CEn ($\sim 135°$) to HT-CEn ($\sim 175°$). The chain angle for HT-CEn is kept smaller than 180°. In the transition from HT-CEn to L-CEn, the degree of kinking increases by being curved by more than 180°. The potential barrier of the reverse change from the expansion to the stretch at 180° is considered to be the cause of stabilization of the metastable phase under ambient conditions. In the transition from L-CEn to HT-CEn, the tetrahedral chain angle of 160° (= −200°: note that the rotation observed by HP-CEn to HT-CEn is the reverse rotation) increases up to 180° with increasing temperature as measured by *in-situ* high-temperature experiments. The angle does not exceed 180° in HT-CEn because contraction of volume is needed. Since the potential barrier on kinking of the silicate tetrahedral chains is not exceeded and the structural change from HT-CEn to L-Cen is quick, HT-CEn-type modifications cannot be frozen without pressure.

3.2. Abnormal bonding distances and displacement ellipsoids in the metastable phase

Table 3 shows the unit-cell dimensions and volumes of enstatite polymorphs and diopside. The molar volume of HT-CEn [30.983 (5) cm^3 mol^{-1}] is between that of HP-CEn at high pressure [28.708 (23) cm^3 mol^{-1} at 7.9 GPa] and those of other pyroxenes at ambient conditions [31.266 (8) cm^3 mol^{-1} for L-CEn, 31.278 (4) cm^3 mol^{-1} for OEn and 32.350 (8) cm^3 mol^{-1} for PEn]. Table 4 indicates the selected interatomic distances for high-temperature CEn, high-pressure CEn (7.9 GPa) and low CEn. The observed average Mg1—O and Si—O distances in HT-CEn (1.997 and 1.620 Å, respectively) are shorter than those in HP-CEn at 7.9 GPa (2.024 and 1.631 Å, respectively; Angel *et al.*, 1992). On the other hand, the average Mg2—O distance in HT-CEn (2.311 Å) is significantly longer than that in L-CEn (2.142 Å; Morimoto *et al.*, 1960), providing an abnormal larger distance for the Mg2 atom. Moreover, the Mg2 polyhedron in HT-CEn, analogous to Ca in diopside, has six O atoms with Mg2—O distances from 2.236 (2) to 2.436 (2) Å and is more irregular than that in HP-CEn. These results indicate that the HT-CEn is the metastable phase transformed from HP-CEn stable at high pressure and high temperature.

In the CIF (supplementary material) and Fig. 3, the Debye–Waller factor and displacement ellipsoids for Mg2, O1, O2 and O3 atoms in HT-CEn have abnormally larger amplitudes (the largest values attain to 0.033 Å^2 from 0.028 Å^2), although those for Mg1 and Si are normal (0.004–0.012 Å^2). The transition mechanism from HP-CEn to HT-CEn is reflected in

Table 4
Selected interatomic distances for high-T CEn, high-P CEn (7.9 GPa; Angel *et al.*, 1992) and low CEn (Morimoto *et al.*, 1960; the names of the sites are unified).

	High-T CEn	High-P CEn	Low CEn
⟨MgO_6 octahedron⟩			
*M*1—O1	2.076 (2)	2.087 (8)	1.985, 2.066
*M*1—O1	1.983 (1)	2.011 (5)	2.030, 2.032
*M*1—O2	1.931 (2)	1.975 (8)	–
*M*1—O3	–	–	2.142, 2.177
Average	1.997	2.024	2.072
*M*2—O1	2.236 (2)	2.067 (8)	2.032, 2.053, 2.279, 2.414
*M*2—O2	2.260 (2)	1.983 (7)	1.985, 2.090
*M*2—O3	2.436 (2)	2.195 (8)	–
Average	2.311	2.082	2.142
⟨SiO_4 tetrahedron⟩			
T—O1	1.621 (1)	1.598 (9)	1.646, 1.615
T—O2	1.582 (2)	1.582 (7)	1.589, 1.586
T—O3	1.636 (2)	1.668 (8)	1.610, 1.676
T—O3	1.640 (2)	1.676 (6)	1.665, 1.676
Average	1.620	1.631	1.628, 1.638

these results. The local coordination environments of Mg1 and Si atoms are maintained during the transition. On the other hand, the anisotropy in the displacement ellipsoids of O2 and O3 atoms is characteristic; the direction of the maximum amplitudes of these atoms is in harmony with the direction of the change in kinking of the tetrahedral chain from HP-CEn to HT-CEn and with the direction of expansion in the Mg2—O3 bonds (Fig. 3). This shows that static irregularity of the atomic displacement caused by the transition is frozen in the metastable state; thus, the history of the structural transition is left in the metastable structure.

3.3. Existence of HP-CEn in nature

In the present study the single crystal of HT-CEn was discovered from the pressure and temperature quench sample achieved by rapidly releasing the oil pressure load and/or by a blow out of the anvil cell gasket from the high-temperature and high-pressure conditions where HP-CEn is stable. The HT-CEn is found ordinarily and abundantly in the pressure- and temperature-quenched sample. As shown previously, we expect that our precise structure analyses provide evidence and a mechanism for the transition from HP-CEn to HT-CEn. The quenching route shown in Fig. 1 is predicted for a blow out of the anvil cell gasket because in this case the descent of pressure is much more rapid than that of temperature; HT-CEn is transformed from HP-CEn during this quenching route. In usual high-pressure and high-temperature experiments, recovery of the synthesized products is performed by releasing pressure slowly after isobaric temperature quenching; pressure quenching is not done because of the danger of the hard metal anvil destruction. L-CEn is recovered in the usual way; HP-CEn transforms to L-CEn by temperature quenching and pressure annealing (Angel & Hugh-Jones, 1994; Angel *et al.*, 1992). In the case of pressure and temperature quenching, our result shows that the metastable HT-CEn can be frozen during passing through the stable area of O-En, and consequently the quenching route shown in Fig. 1 obstructs the spontaneous transition to L-CEn.

When the cooling rate and quenching route are satisfied, HT-CEn is quenched as a metastable structure formed at the middle stage of the transition from HP-CEn to L-CEn. This type of metastable HT-CEn may be found in natural rocks that had rapid quenching history such as a shock-metamorphosed meteorite, although its actual appearance depends on the kinetic factors such as the quenching rate of pressure and temperature or duration of stay at a particular temperature. The occurrence of HT-CEn converted from HP-CEn indicates that rocks including it have experienced extreme high pressure and temperature, and simultaneous quenching of pressure and temperature with rapid rate. To date, L-CEn has been found in meteorites (Price *et al.*, 1979) and ultra high-pressure metamorphic rocks (Bozhilov *et al.*, 1999). However, we anticipate finding metastable HT-CEn converted from HP-CEn, instead of LT-CEn, in shocked enstatite chondrites and bronzite chondrites; HT-CEn should be more stabilized by a small substitution of larger Ca (diopside component) because the *M*2 site is too large for Mg. Tribaudino *et al.* (2005) show experimental evidence in synthetic L-CEn with a diposide component. Furthermore, our X-ray diffraction experiments show that the HT-CEn structure breaks easily with shear stress. We would like to report decomposition of the metastable phase in detail in another paper together with the results of Raman spectrum measurements. In order to preserve the metastable thermodynamic history record, it is necessary to avoid making powder and thin sections, and to deal with the single crystals carefully.

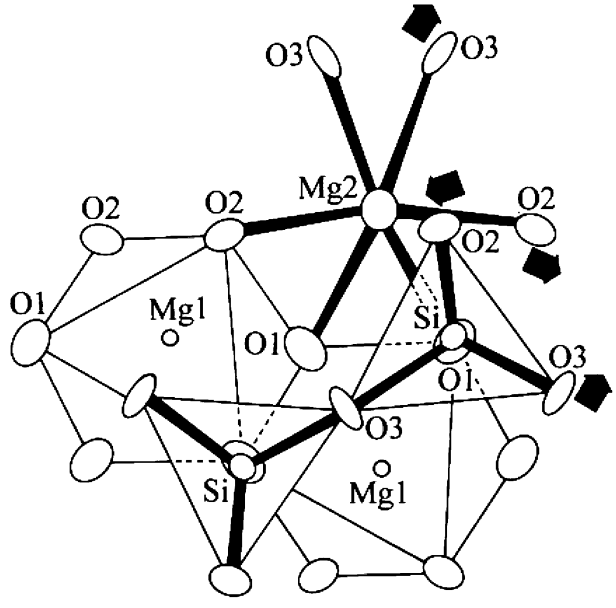

Figure 3
The displacement ellipsoids of Mg1, Mg2, Si, O1 and O2 atoms in HT-CEn projected on (100). Atoms are drawn at the 50% probability level.

References

Akaogi, M. & Akimoto, S. (1977). *Phys. Earth Planet. Inter.* **15**, 90–106.

Alvaro, M., Cámara, F., Domeneghetti, M. C., Nestola, F. & Tazzoli, V. (2011). *Contrib. Mineral. Petrol.* **162**, 599–613.

Alvaro, M., Nestola, F., Ballaran, T. B., Camara, F., Domeneghetti, M. C. & Tazzoli, V. (2010). *Am. Mineral.* **95**, 300–311.

Angel, R. J., Chopelas, A. & Ross, N. L. (1992). *Nature*, **358**, 322–324.

Angel, R. J. & Hugh-Jones, D. A. (1994). *J. Geophys. Res.* **99**, 19777–19783.

Arlt, T. & Armbruster, T. (1997). *Eur. J. Mineral.* **9**, 953–954.

Bowen, N. L. & Schairer, J. F. (1935). *Am. J. Sci.* **29**, 151–217.

Bozhilov, K. N., Green, H. W. & Dobrzhinetskaya, L. (1999). *Science*, **284**, 128–132.

Cámara, F., Carpenter, M. A., Domeneghetti, M. C. & Tazzoli, V. (2002). *Phys. Chem. Miner.* **29**, 331–340.

Cámara, F., Iezzi, G. & Oberti, R. (2003). *Phys. Chem. Miner.* **30**, 20–30.

Cameron, M., Sueno, S., Prewitt, C. T. & Papike, J. J. (1973). *Am. Mineral.* **58**, 594–618.

Christy, A. G. (1995). *Acta Cryst.* B**51**, 753–757.

Dera, P., Finkelstein, G. J., Duffy, T. S., Downs, R. T., Meng, Y., Prakapenka, V. & Tkachev, S. (2013). *Phys. Earth Planet. Inter.* **221**, 15–21.

Gasparik, T. (1990). *Am. Mineral.* **75**, 1080–1091.

Iishi, K. & Kitayama, H. (1995). *Neues Jahrb. Miner. Monatsh.* **2**, 65–74.

Ito, E. & Takahashi, E. (1987). *High-Pressure Research in Mineral Physics*, edited by M. H. Manghnani & Y. Syono, pp. 221–230. Tokyo: Terra Scientific Publishing Company.

Jahn, S. (2008). *Am. Mineral.* **93**, 528–532.

Jiang, D., Fujino, K., Tomioka, N., Hosoya, T. & Das, K. (2002). *J. Mineral. Petrol. Sci.* **97**, 20–31.

Kawai, N., Togaya, M. & Onodera, A. (1973). *Proc. Jpn Acad.* **49**, 623–626.

Momma, K. & Izumi, F. (2006). *Commission on Crystallographic Computing Newsletter*, No. 7, pp. 106–119.

Morimoto, N., Appleman, D. E. & Evans, H. T. (1960). *Z. Kristallogr.* **114**, 120–147.

Murakami, T., Takéuchi, Y. & Yamanaka, T. (1984). *Z. Kristallogr.* **166**, 263–275.

Nakatsuka, A., Yoshiasa, A., Yamanaka, T. & Ito, E. (1999). *Am. Mineral.* **84**, 199–202.

Nakatsuka, A., Yoshiasa, A., Yamanaka, T., Katsura, T. & Ito, E. (1999). *Am. Mineral.* **84**, 1135–1143.

Ohashi, Y. (1984). *Phys. Chem. Miner.* **10**, 217–229.

Presnall, D. C. & Gasparik, T. (1990). *J. Geophys. Res.* **95**, 15771–15777.

Price, G. D., Putnis, A. & Agrell, S. O. (1979). *Contrib. Mineral. Petrol.* **71**, 211–218.

Redhammer, G. J., Cámara, F., Alvaro, M., Nestola, F., Tippelt, G., Prinz, S., Simons, J., Roth, G. & Amthauer, G. (2010). *Phys. Chem. Miner.* **37**, 658–704.

Redhammer, G. J. & Roth, G. (2004). *Z. Kristallogr.* **219**, 585–605.

Rigaku Corporation (1999). *WinAFC*, Version 1.03. Rigaku Corporation, Tokyo, Japan.

Ringwood, A. E. (1967). *Earth Planet. Sci. Lett.* **2**, 255–263.

Sasaki, S. (1987). *KEK Internal Report 5.*

Shimobayashi, N. & Kitamura, M. (1991). *Phys. Chem. Miner.* **18**, 153–160.

Shimobayashi, N. & Kitamura, M. (1993). *Mineral. J.* **16**, 416–426.

Shimobayashi, N., Miura, E. & Miyake, A. (1998). *Proc. Jpn Acad.* **74**, 105–109.

Smyth, J. V. (1969). *Nature*, **222**, 256–257.

Smyth, J. R. (1974). *Am. Mineral.* **59**, 1069–1082.

Tribaudino, M., Nestola, F., Cámara, F. & Domeneghetti, M. C. (2002). *Am. Mineral.* **87**, 648–657.

Tribaudino, M., Nestola, F. & Meneghini, C. (2005). *Can. Mineral.* **43**, 1411–1421.

Yoshias, A. (2001). *J. Cryst. Soc. Jpn*, **43**, 297–305.

Yusa, H., Akaogi, M. & Ito, E. (1993). *J. Geophys. Res.* **98**, 6453–6460.

Zhang, J. S., Dera, P. & Bass, J. D. (2012). *Am. Mineral.* **97**, 1070–1074.